PCCP

Physical Chemistry Chemical Physics

Accepted Manuscript

This is an Accepted Manuscript, which has been through the Royal Society of Chemistry peer review process and has been accepted for publication.

Accepted Manuscripts are published online shortly after acceptance, before technical editing, formatting and proof reading. Using this free service, authors can make their results available to the community, in citable form, before we publish the edited article. We will replace this Accepted Manuscript with the edited and formatted Advance Article as soon as it is available.

You can find more information about Accepted Manuscripts in the Information for Authors.

Please note that technical editing may introduce minor changes to the text and/or graphics, which may alter content. The journal's standard Terms & Conditions and the Ethical guidelines still apply. In no event shall the Royal Society of Chemistry be held responsible for any errors or omissions in this Accepted Manuscript or any consequences arising from the use of any information it contains.

ARTICLE

Triplet state structure-property relationships in a series of platinum acetylides: effect of chromophore length and end cap electronic properties

Received 00th January 20xx,
Accepted 00th January 20xx

DOI: 10.1039/x0xx00000x

Thomas M. Cooper,*[a] Joy E. Haley,[a] Douglas M. Krein,[b] Aaron R. Burke,[b] David J. Stewart,[b] Jennifer L. Fore[c] and Jonathan E. Slagle[a]

To develop quantitative structure–spectroscopic property relationships in platinum acetylides, we investigated the triplet state behavior of nominally centrosymmetric chromophores *trans*-Pt(PBu3)$_2$(C≡C-Phenyl-**X**)$_2$, where **X** = diphenylamino, NH_2, OCH_3, t-Bu, CH_3, H, F, benzothiazole, CF_3, CN, and NO_2. We measured ground state absorption, phosphorescence, excitation spectra, triplet state absorption spectra and triplet lifetimes. By DFT we calculated the phosphorescence emission energy(E_T), the spin density on the end cap(SD(**X**)), triplet state geometry and the distance between the triplet centroid and the central platinum atom($<R_{S\text{-}Pt(X)}>$). Compounds with electron-donating **X** have smaller triplet state lifetime, blue-shifted phosphorescence and larger triplet potential energy surface displacement associated with the C≡C bond. Compounds with electron-withdrawing **X** have larger triplet lifetime, red-shifted phosphorescence and smaller triplet potential energy surface displacement associated with the C≡C bond. The range of spin-orbit-coupling between the platinum atom and the triplet centroid was determined to be 6 Å. The quantity $<R_{S\text{-}Pt}>$ is shown to be a linear function of one-dimensional well length calculated from experimental E_T. The multiple examples demonstrate $<R_{S\text{-}Pt}>$ is a useful descriptor for analyzing triplet state behavior.

Introduction

Two-photon absorbing(2PA) and effective three photon**(E3PA)** absorbing materials have utility in a variety of nonlinear photonics applications.[1-3] Good 2PA chromophores have been found to have either an asymmetrical D-π-A (donor- π -conjugated group-acceptor) or a symmetrical D-π-A-π-D or A-π-D-π-A structural motif leading to a large change in polarization upon excitation.[4,5] Platinum acetylides have been intensively studied as nonlinear optical materials.[6-8] We have investigated platinum acetylide 2PA and E3PA chromophores possessing both the asymmetrical and symmetrical structural motif. In particular, we measured a large two photon cross section in the A-π-D-π-A chromophore E1-BTF.[2] E1-BTF behaves as an E3PA chromophore, having both a large 2PA cross section and strong spin-orbit-coupling(SOC) from the central Pt atom giving efficient conversion to the triplet state.

To develop quantitative-structure-property relationships(QSPR) for E1-BTF-like chromophores, we have published a series of papers focusing on 2PA and time-resolved spectroscopy.[9-11] We designed two series of platinum-acetylide complexes to determine effects of ligand length: H-π_1-π_2-**X** *vs.* H-π_2-**X** and end cap **X** acceptor electronic properties: electron-donating(ED) *vs.* electron-withdrawing(EW) on 1PA, 2PA and excited-state spectra. The end caps(**X**) are listed in Chart 1. The first series we published was the **X**-π_2-π_1-Pt(PBu$_3$)$_2$-π_1-π_2-**X** chromophore *trans*–bis-(tributylphosphine)-bis-(4-((9,9-diethyl-7-ethynyl-9H-fluoren-2-yl)ethynylphenyl)-platinum, designated as "**Fl-X**", where we measured time-resolved spectroscopy, triplet state behavior and 2PA spectra.

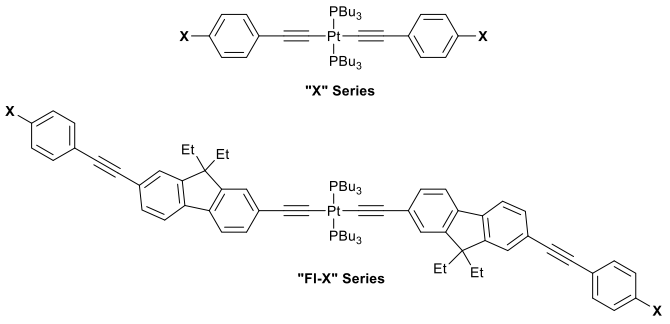

Chart 1 Molecular formula of platinum acetylide "**X**" series **X**-π_2-Pt(PBu$_3$)$_2$-π_2-**X** series; π_2 = phenyl acetylene(PA); Also presented is "**Fl-X**" series X-π_2-π_1-Pt(PBu$_3$)$_2$-π_1-π_2-X; DPA=diphenyl amino; BTH=benzothiozole.

[a] *Materials and Manufacturing Directorate, Air Force Research Laboratory, Wright-Patterson Air Force Base, OH 45433.*
[b] *General Dynamics Information Technology, Dayton, OH 45431.*
[c] *SOCHE Student Research Program, Dayton, OH 45420.*

[d] *Electronic Supplementary Information (ESI) available: Phosphorescence emission and excitation spectra of samples dissolved in Me-THF glasses, triplet state absorption spectra obtained from flash photolysis are and DFT calculation results. See DOI: 10.1039/x0xx00000x*

DFT calculations show relationships between the ligand spin distribution and triplet state lifetimes and phosphorescence quantum yields. We measured the instantaneous 2PA spectra of the **Fl-X** series[12] and the ligands.[13] DFT calculations show low-energy-cost ligand distortion to out-of-plane conformations yielding 2PA cross sections calculated from a S_1 state two-level model that agree with experiment. Due to out-of-plane ground state conformations, the **Fl-X** S_1 state has D-π-A character rather than MLCT character expected from the nominally centrosymmetric A-π-D-π-A formula. Measurement of 2PA by both nonlinear absorption and fluorescence of the complexes and ligands shows the complexes have E3PA behaviour arising from $S_1 \rightarrow S_n$ transitions as well as the $S_0 \rightarrow S_1$ transition.

The second series is the **X**–π_2-Pt(PBu_3)$_2$-π_2-**X** chromophore trans-bis(tributylphosphine)bis(ethynylphenyl)-platinum, labeled "**X**"(Chart 1). We recently published 1PA and 2PA spectra for the **X** series.[14] TDDFT calculations from energetically and statistically favorable out-of-plane conformations predict 1PA transition dipoles and 2PA cross sections agreeing with experiment.

In the current work we present triplet state data from series **X**. We use DFT calculations to explain the effect of end cap **X** on triplet state behavior and QSPRs. We tested descriptors including calculated triplet energy, triplet-versus-singlet-state geometry changes, end cap spin density and spin-weighted average distance between the triplet centroid(TC) and the central platinum atom. Good correlations were found between these descriptors and measured phosphorescence energy, Huang-Rhys factors and triplet-state-lifetime data. These descriptors are useful as a starting point for higher level calculations[15] and machine learning studies of large chromophore sets.[11,16]

Experimental and computational methods

Chromophore synthesis and spectroscopic methods have been published.[1,14] Ground state absorption spectra of these compounds dissolved Me-THF, emission and excitation spectra were collected from Me-THF glass at 77 K. Emission spectra(10 nm ex/em slit width) were obtained by exciting the sample at the absorption maximum while excitation spectra(10 nm ex/em slit width) were obtained by monitoring emission intensity at the emission maximum. The spectra corrected for inner filter effect and converted to transition dipole moment representation[17] are shown in Fig 1 and S1 – S11.

Room temperature triplet state absorption spectra and lifetimes were measured by laser flash photolysis. A detailed description of the laser flash photolysis apparatus was published earlier.[18] The samples were dissolved in benzene and deoxygenated by three successive freeze-pump-thaw cycles. Nanosecond-transient-absorption measurements were carried out using the third harmonic (355 nm) of a Q-switched Nd:YAG laser (Quantel Brilliant, pulse width of ~5 ns). Pulse fluences of up to 1 mJ cm^{-2} at the excitation wavelength were typically used.

Room temperature ultrafast transient absorption spectra were performed using a modified version of the femtosecond pump-probe UV-VIS spectrometer.[19] We obtained 1 mJ, 150 fs pulses at 800 nm at 1 kHz repetition rate from a diode-pumped, Ti:Sapphire regenerative amplifier (Spectra Physics Hurricane). The output laser beam was split into pump and probe (85 and 15%) by a beam splitter. The pump beam was directed into a frequency doubler (CSK Super Tripler) and then was focused into the sample. The probe beam was delayed in a computer-controlled optical delay (Newport MM4000 250 mm linear positioning stage) and then focused into a sapphire plate to generate white light continuum. The white light was then overlapped with the pump beam in a 2 mm quartz cuvette and then coupled into a CCD detector (Ocean Optics S2000 UV-VIS). Data acquisition was controlled by software developed by Ultrafast Systems LLC.

DFT calculations were done using Gaussian 09W, Version 7.0.[20] The chromophores were modeled as *trans*-Pt(PMe_3)$_2$(CC-Phenyl-**X**)$_2$. The THF solvent environment was simulated with the polarizable continuum model.[21] We performed DFT energy minimizations for the ground and triplet state using B3LYP/6-311g(2d,p). Excited state TDDFT calculations of the $S_0 \rightarrow S_1$ and $S_0 \rightarrow T_1$ transitions used CAM-B3LYP/6-311g(2d,p). CAM-B3LYP has long range corrections that give more accurate excited state energies, especially for charge transfer transitions.[22] The basis set for the central Pt atom was SDD. We obtained excited state population densities using the default "Pop = Orbitals = 5" keyword. We performed relaxed potential energy surface(PES) scans on the S_0 and T_1 state of **H** by varying the dihedral angle between the two phenyl rings from 0 to 90 deg and minimizing the energy with frozen dihedral angle. We calculated the phosphorescence 0-0 band energy from the expression

$$E(T_1\text{-}S_0) = E_{T1}(T_1 \text{ geometry} - E_{S0}(T_1 \text{ geometry}) \quad (1)$$

Atomic spin density differences between the α and β occupied orbitals were obtained from the default calculation output.

Results and discussion

Table 1 summarizes the spectroscopic data for series X. Figs. 1A, 1B and 1C show ground state absorption, emission and excitation spectra, respectively. Ground state absorption spectra were published previously and shown for reference.[14] Fluorescence is weak(ϕ_f(BTH) = 0.018, ϕ_f < 0.004 for all other compounds). Previously we measured the room temperature phosphorescence quantum yield of H to be ϕ_p = <0.0001.[18] The room temperature phosphorescence quantum yields of the Fl-X series are also a few percent. Because of the low yields of the other systems, we did not measure room temperature phosphorescence quantum yields in the current series and consider triplet decay to be mostly nonradiative. We measured triplet state absorption spectra and lifetimes(Table 1, Figs S13-S18). The data for NH_2 and CF_3 had a poor signal-to-noise ratio due to their lifetimes being less than the 100 ns time resolution limit of the instrument.

ARTICLE

Table 1 Spectroscopic data

X	λ_{max}(GS)[a]	λ_{max}(ph)[b]	S[c]	λ_{max}(ex)[d]	ΔE_{ST}[e]	$T_1T_{n\ max}$[f]	τ_T[g]	V_{SOC}[i]
NH_2	341(2.99)	462	0.597	361	0.751	Small signal	<100 ns	--
OCH_3	332(2.81)	442	0.637	344	0.799	---	---	---
DPA	356(6.91)	486	0.583	380	0.712	750	420(52) ns	0.762
t-Bu	326(2.87)	438	0.644	341	0.805	---	---	---
CH_3	327(3.04)	442	0.639	343	0.810	---	---	---
H	323(2.58)	439	0.624	342	0.807	626	590(150) ps	30.3
F	323(2.53)	435	0.686	338	0.818	---	---	
BTH	377(11.0)	542	0.570	403	0.793	610	183(33) μs	0.0247
CF_3	326(3.00)	449	0.658	349	0.791	Small signal	<100 ns	--
CN	335(4.84)	476	0.620	367	0.779	670	331(39) ns	0.920
NO_2	386(5.19)	530	---	425	0.582	740	19(2) μs	0.0828

[a]All wavelengths in nm; Ground state absorption spectrum maximum; quantity in parenthesis is extinction coefficient($M^{-1}cm^{-1}$) x 10^{-4}.

[b]Wavelength of 0-0 band from phosphorescence spectra obtained from Me-THF glass at 77 K.

[c]Huang-Rhys parameter for C≡C vibration(~2,000 cm^{-1}) equaling the square root of the emission spectrum intensity relative to the 0-0 band. No band was observed on **NO_2**. The uncertainty is estimated to be 3% from instrumental noise.

[d]Wavelength of 0-0 band from phosphorescence excitation spectra obtained from Me-THF glass at 77 K.

[e]$\Delta E_{ST}(eV) = E_{ex} - E_{em}$ obtained from excitation and emission spectra 0-0 bands.

[f]Triplet state absorption spectrum maximum. Due to blue-shifted absorption spectra we were unable to collect spectra from **OCH_3**, **t-Bu**, **CH_3** and **F**.

[g]Triplet lifetime with standard deviation in parenthesis obtained from samples dissolved in benzene and deoxygenated by freeze pump thaw. Triplet spectrum and lifetime of compound **H** previously published.[23]

[h]Electronic coupling energy V_{SOC}(meV) between T_1 and S_0 states calculated from equation (7).

ARTICLE

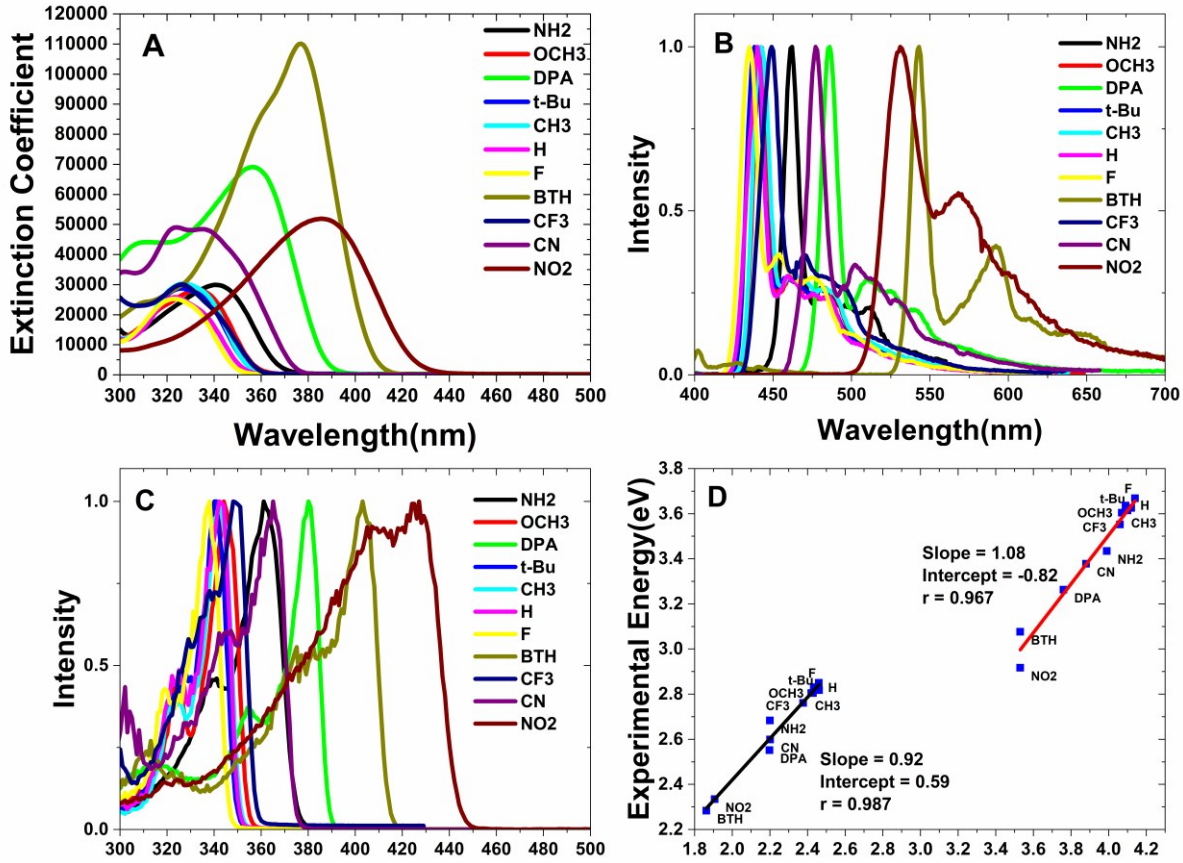

Fig. 1 Spectra of series **X** obtained from Me-THF solution. A: Ground state absorption spectra obtained from solution at room temperature; B: Emission spectra from Me-THF glass at 77 K; C: Excitation spectra from Me-THF solution at 77 K; D: Plot of experimental 0-0 band transition energies(Table 1) obtained from emission and excitation spectra at 77 K *vs.* calculated emission($T_1 - S_0$) and excitation($S_0 - S_1$) spectra transition energies(Table 2).

ARTICLE

We normalized the phosphorescence(Fig. 2) and excitation(Fig. 3) spectra to the 0-0 band. The phosphorescence and excitation spectra show strong 0-0 bands and weaker vibronic peaks. This bandshape is typical of phenyl acetylenes and platinum acetylides due to nearly diagonal Duschinsky matrix and small excited state potential energy surface displacement(ΔPES).[6,24,25] The excitation and emission spectra contain information about the process of instantaneous excitation of the equilibrium ground state to the FC S_1 state, followed by relaxation to the equilibrium T_1 state and FC emission to the ground state having equilibrium T_1 state conformation. Both the excitation and emission spectra have very clear 0-0 bands, so ΔE_{ST} can be measured.

The 0-0 bands of the excitation spectra are broader than those of the emission spectra, suggesting the ground state PES is flatter than the excited state PES. All the spectra presented in the upper panel of Fig 1 show similar band shape with vibronic peaks near 1,000 cm^{-1} and 2,000 cm^{-1}. In particular, the 2,000 cm^{-1} band is associated with C≡C stretch vibrations. To estimate triplet state ΔPES relative to the ground state, we estimated the Huang-Rhys factor S from the intensity of the 2,000 cm^{-1} band. The lower panel of Fig 2 shows phosphorescence spectra for **BTH** and **NO_2**. **BTH** and **NO_2** show vibronic bands at 1,550 cm^{-1} and 1,300 cm^{-1} associated with the benzothiazole and nitro portions of the ligand, respectively.

A comparison of the emission(Fig. 2) with the excitation spectra(Fig. 3) bandshapes gives insight into the conformation distribution of the FC S_1 state compared to the equilibrium T_1 state. The excitation spectra in the upper panel of Fig. 2 have broad vibronic peaks near 1,700 cm^{-1}. The lower frequency compared to the emission spectra gives evidence for bond length differences between the S_1 and equilibrium T_1 states. The 0-0 bands of the excitation spectra are broader than those of the emission spectra, suggesting a broad ground state and narrower T_1 state conformation distribution. The excitation spectra of **BTH** and **NO_2** in the lower panel of Fig. 3 are broader than the corresponding emission spectra(Fig. 2), which show distinct vibronic bands. The differences between excitation and emission spectra suggest excitation to the S_1 state from a disordered ground state conformation distribution followed by relaxation into a more ordered equilibrium T_1 state conformation distribution. In particular, the emission spectra of **BTH** and **NO_2** suggest the triplet state is located on benzothiazole and nitro groups having ordered conformation.

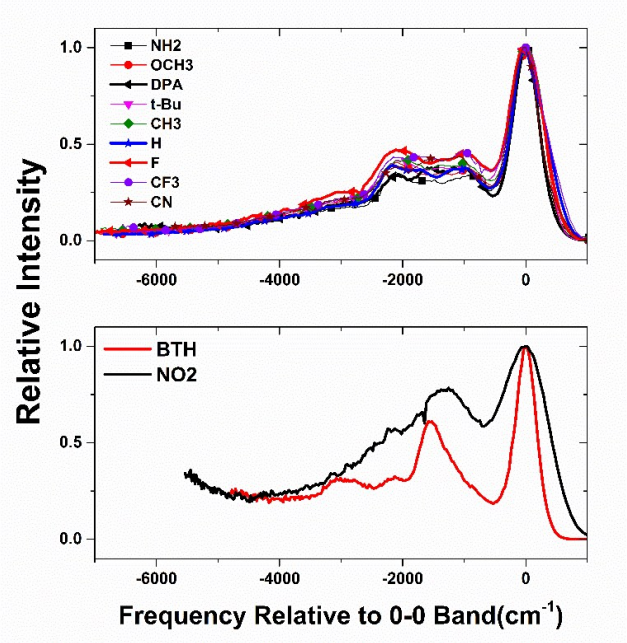

Fig. 2 Emission spectra of series **X** relative to 0-0 band obtained from Me-THF glass at 77 K.

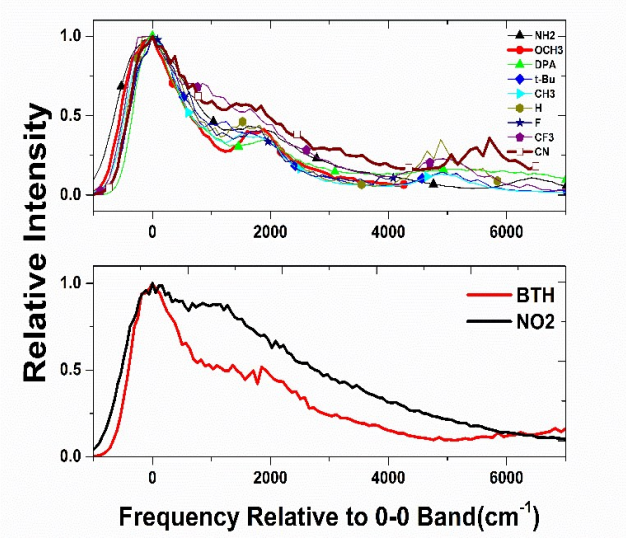

Fig. 3 Excitation spectra of series **X** relative to 0-0 band obtained from Me-THF glass at 77 K.

Similar behavior has been observed in the fluorescence of phenyl acetylene oligomers.[26,27]

ARTICLE

Table2 Data from DFT calculations

Ligand(**X**)	SD(**X**)[a]	ΔR_{RMS}(PA)[b]	ΔR_{RMS}(**X**)[c]	$<R_{S\text{-}Pt}>$[d]	$\Delta\rho$[e]	μ_T[f]	$\Delta\mu_{01}$[g]	E_T[h]	E_{T1}[i]	n_π[j]
NH_2	0.197	0.041	0.0013	4.50	0.35	2.33	2.98	2.37	2.84	10
OCH_3	0.107	0.044	0.0019	4.35	0.28	0.07	1.3	2.43	2.90	8
DPA	0.338	0.041	0.0058	5.38	0.23	2.53	4.45	2.20	2.67	22
t-Bu	0.003	0.042	0.0043	4.29	0.18	1.67	0.53	2.43	2.90	8
CH_3	0.011	0.044	0.011	4.31	0.18	1.67	0.74	2.42	2.89	8
H	-0.036	0.043	0.000	4.13	0.18	2.11	-0.07	2.46	2.92	8
F	0.040	0.043	0.0005	4.17	0.16	1.73	0.5	2.46	2.93	8
BTH	0.636	0.032	0.022	6.58	-0.20	6.13	3.69	1.86	2.35	18
CF_3	0.032	0.040	0.012	4.34	-0.06	4.35	2.69	2.38	2.81	8
CN	0.157	0.040	0.022	4.91	-0.15	5.30	5.24	2.20	2.60	10
NO_2	0.484	0.031	0.049	5.42	-0.26	14.0	10.1	1.91	2.46	12

[a]Spin density on end cap(**X**) of the ligand calculated from equilibrium T_1 geometry.

[b]RMS phenyl acetylene(PA) bond length change T_1 state *vs.* ground state(Å)

[c]RMS end cap bond length change T_1 state *vs*. ground state(Å)

[d]Spin-weighted average distance between TC and central platinum atom(Å).

[e]Population change on Pt calculated from population analysis of S_1 state when platinum complex is in an out-of-plane conformation. Change in population is defined as population(π* orbital, platinum atom) – population(d orbital, platinum atom).

[f]T_1 state dipole moment(D) calculated from equilibrium T_1 geometry.

[g]Dipole moment difference(D) between S_1 state and ground state previously published.[3]

[h]E_T = E_T(equilibrium T_1 geometry) – E(S_0, equilibrium T_1 geometry)(eV). The equilibrium T_1 geometry was calculated from a DFT energy minimization.

[i]Franck-Condon T_1 energy(eV) calculated from TDDFT calculation on the equilibrium S_0 geometry

[j]Number of π electrons on the X series ligand. For **Fl-X** series, add 14 π electrons.

Table 2 summarizes the DFT calculation results. For all the complexes, the lowest energy conformations for both S_0 and T_1 states has coplanar phenyl rings. To estimate the barrier to rotation about the phenyl acetylene bond we did a PES scan on **H**. The rotation barrier about the phenyl acetylene bond is ~0.4 kcal/mole(0.015 eV) for the S_0 state and ~0.3 kcal/mole(0.01 eV) for the T_1 state(Fig. S12). The rotation barrier is slightly larger for the S_0 state than the T_1 state due to resonance from delocalized S_0 state *vs.* confinement of the T_1 state to the ligand. Fig. S12 gives the calculated Boltzmann-weighted fraction as a function of dihedral angle at both room temperature and 77 K. Although the planar conformation is favored at low temperature, there is still a broad distribution of nonplanar conformations both at room temperature and 77 K. In previous calculations we assumed the 90 deg dihedral angle between the two phenyl groups and calculated 1PA $S_0 - S_1$ transition dipoles, energies and 2PA cross sections in good agreement with experiment.[14] The calculated T_1 emission energies assume a relaxed planar T_1 state conformation. However, the rotation barrier about the phenyl rings is ~0.01 eV, so the conformation has a small effect on the calculated T_1 state emission energy (E_T~2-3 eV). Because of the low rotation barrier, there will be a distribution of molecular conformations in all cases. Comparison of the excitation and emission spectra of **NO_2** and **BTH** (Figs. 2 and 3) suggest the T_1 state has a more structured PES localized on the ligand not influenced by the dihedral angle between the two phenyl groups.

Fig. 1D shows plots of experimental *vs.* calculated S_1 and T_1 energies. The linear regressions for both excitation and emission spectra have near unity slope, but there are offsets in the intercepts due to factors such as basis set, functional and the use of the polarizable continuum model. Inclusion of conformation-

distribution effects by sampling conformations obtained from molecular dynamics methods followed by statistical averaging would improve the calculated state energies.[28]

In order to interpret phosphorescence spectra band shape, we analyzed the relation between equilibrium T_1 state spin densities and geometry. All the data for this analysis can be found in the electronic supplementary information(Tables S1-S7). Table S7 gives images for the HOMO, LUMO and T_1 state spin density for series **X**. Chart 2 shows an example image set for **BTH**. The images show that the out-of-plane conformation results in the HOMO and LUMO being confined to one ligand plus the platinum atom. The equilibrium T_1 state spin density is also confined to one ligand.

We performed a population analysis(Table2, Table S5) of the S_1 state. The S_1 state is a mixture of a $d\pi^*$ transition on the platinum atom and $\pi\pi^*$ transition on the ligand. The change in electron density between the S_1 state and the ground state($\Delta\rho=\rho(\pi^*)-\rho(d)$) on the platinum atom measures the CT character. The density change correlates with ligand electron affinity(EA)(Fig. 4 upper panel). When the ligand has a small EA, e.g. **NH_2**, **OCH_3** and DPA, $\Delta\rho > 0$ and the S_1 state has LMCT character. The moderate LMCT S_1 states of compounds **H**, **F**, **CH_3**, and **t-Bu** have $\Delta\rho \sim 0.16 - 0.18$. When the ligand has large EA, e.g. **BTH**, **CN** and **NO_2**, $\Delta\rho < 0$ and the S_1 state has MLCT character. The S_1 state of **CF_3**($\Delta\rho$ = -0.03) has intraligand(IL) character.

The relation between *SD(**X**)* and S_1 state charge densities are shown in the lower panel of Fig. 4. It gives the relation between instantaneous charge movement upon excitation to the S_1 state and the end cap spin density in the equilibrium T_1 state. The fitted curve is a concave-upward quadratic function. Compounds **NO_2**, **BTH**, **CN** have $\Delta\rho < 0$ and slope < 0 associated with MLCT states. The T_1 states of **BTH** and **NO_2** have biradicaloid character, with approximately one electron on phenyl acetylene(PA) and another on the end cap. Compounds **H** and **CF_3** are near the minimum, slope ≈ 0, where SD(**X**) < 0.1 and are associated with weak CT to IL S_1 state. The smallest SD(**X**) is seen in compound **H** where two electrons are localized on the PA group. The compounds **F**, **CH_3**, **t-Bu**, **DPA**, **OCH_3** and **NH_2** have $\Delta\rho > 0$, slope > 0 associated with LMCT states.

The spin density is mostly confined to one ligand with the spin density distributed between the platinum atom, the PA unit and the end cap **X**(Table S6).

$$\mathrm{SD(Pt)} + \mathrm{SD(PA)} + \mathrm{SD(X)} \approx 2 \qquad (2)$$

The calculated spin density in the remainder of the molecule ranges from 0.13 (**NH_2**) to 0.03(**BTH**).

We calculated the spin-weighted average distance between the TC and the central platinum atom

$$\langle R_{S-Pt} \rangle = \frac{1}{2}\sum_{atoms} S_i r_{i,Pt}, \qquad (3)$$

where S_i is the spin density on atom i having a distance $r_{i,Pt}$ from the central platinum atom. It is a measure of the triplet dimension and models the triplet state as a point at distance $<R_{S\text{-}Pt}>$ from the central platinum atom. Similar descriptors have been described.[29] *SD(**X**)* is a linear function of $<R_{S\text{-}Pt}>$*(Å)*.

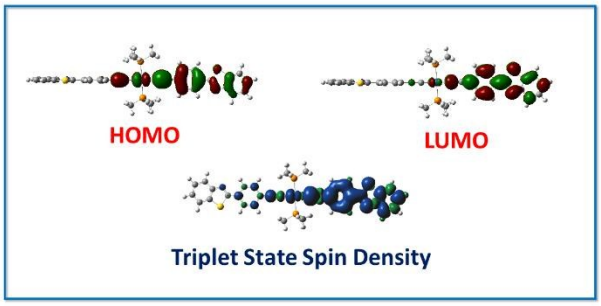

Chart 2 Example images of HOMO, LUMO and triplet state spin density for compound **BTH**. The images for the remaining complexes are given in Table S7.

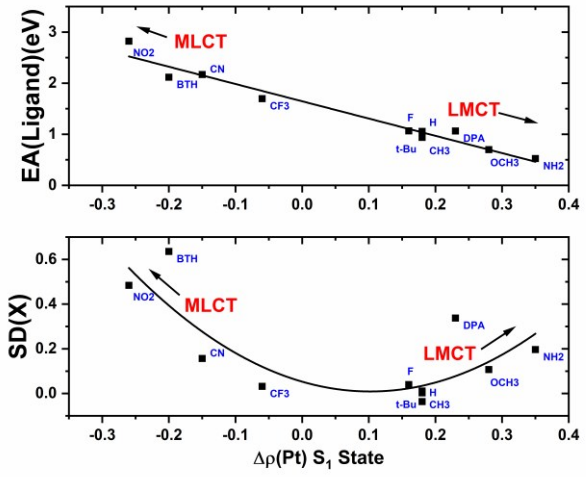

Fig. 4 Upper panel: plot of calculated ligand electron affinity *vs.* difference in electron density between the S_1 state and the ground state($\Delta\rho=\rho(\pi^*)-\rho(d)$) on the platinum atom; lower panel: plot of calculated equilibrium T_1 state spin density on the ligand end cap(SD(**X**)) *vs.* difference in electron density between the S_1 state and the ground state($\Delta\rho=\rho(\pi^*)-\rho(d)$) on the platinum atom.

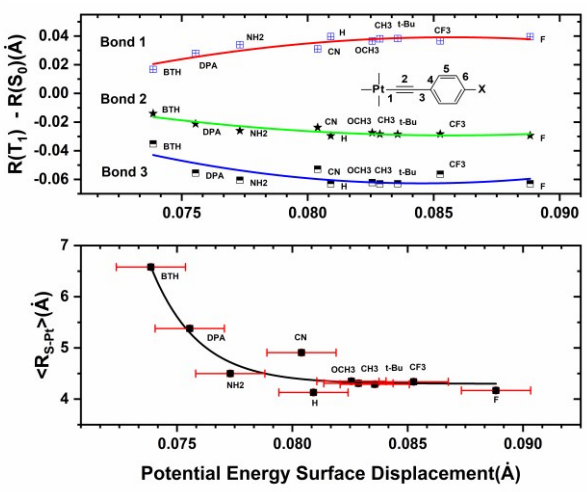

Fig. 5 Upper panel: Plot of bond length change($\Delta R = R(T_1) - R(S_0)$) state vs distance between TC and central platinum atom; Lower panel: plot of T_1 state spin density on the ligand end cap vs. distance between TC and central platinum atom.

$$SD(\mathbf{X}) = -1.14 + 0.291\langle R_{S-Pt} \rangle \quad r = 0.95 \qquad (4)$$

This relation connects the spin density distribution and T_1 state geometry. Compared to *SD(**X**)*, the spin-weighted average distance $\langle R_{S\text{-}Pt}\rangle$ is more general and can be used to compare systems with different classes of ligands, while *SD(**X**)* is specific to series **X**. Bond length changes in PA are a function of $\langle R_{S\text{-}Pt}\rangle$ (upper panel Fig. 5). The PA distortion occurs in bonds 1-4, with no systematic variation in bonds 5 and 6. More distortion is seen in ED end caps, as the spin is localized in PA. With EW end caps, especially **NO_2** and **BTH**, spin density is localized on the end cap so the bond length change is smaller.

Examination of previously published calculated and experimental triplet state behavior of the **Fl-X** series makes possible determination of the effect of the extended conjugation of the fluorenyl group on spectroscopic behavior.[1] In Chart 3 we show $\langle R_{S\text{-}Pt}\rangle$ distances for **X** and **Fl-X**. The quantity $\langle R_{S\text{-}Pt}\rangle$ varies from 4.1 Å in **H** to 6.6 Å in **BTH**. We previously calculated $\langle R_{S\text{-}Pt}\rangle$ for the **Fl-X** series. The values range from ~8 to 15 Å, with the largest (15 Å) in **Fl-BTH**. There is potential difference with current calculations as the previous calculations used the LANL2DZ basis set.

Our previous work and has shown the triplet state is confined to one ligand.[9,30] The effective length of a one-dimensional well relates to state energy and the number of π electrons according to the expression[31]

$$L_{1D} = \sqrt{\frac{h^2}{8m}\frac{n_\pi/2+1}{\Delta E}} \quad , \qquad (5)$$

where n_π is the number of π electrons in one ligand and ΔE is the transition energy E_T. Equation (5) describes optical transitions in a one-dimensional confined well and predicts $1/L^2$ dependence in diphenyl polyenes,[32] colloidal quantum dots,[33,34] F-centers in alkali halides[35] and quantum wells.[36]

We plotted the L_{1D} obtained from experimental E_T *vs.* $\langle R_{S\text{-}Pt}\rangle$, combining the **X** and **Fl-X** series(Fig. 6). In the **X** series, $L_{1D} \sim 2\langle R_{S\text{-}Pt}\rangle$, showing more confinement of the triplet state compared to a one-dimensional well. In the **Fl-X** series, $L_{1D} \sim 9 + 0.5\langle R_{S\text{-}Pt}\rangle$, the slope showing inclusion of fluorenyl spacer group causes less end cap effect as the TC is further away from the central platinum atom. The slope will likely approach zero in larger systems. For **DPA** in both series, $\langle R_{S\text{-}Pt}\rangle \ll L_{1D}$, due to the nonlinear shape of the diphenyl amine ligand compared to the other ligands. The current work shows $\langle R_{S\text{-}Pt}\rangle$ describes confined triplet state dimension and is a linear function of L_{1D}.

Excitation to the S_1 state followed by relaxation to the equilibrium T_1 state involves charge movement as well as bond length changes. Fig. 7 is a plot of ΔE_{ST} *vs.* $\mu_T - \Delta\mu_{01}$. The quantity $\mu_T - \Delta\mu_{01}$ is a measure of the net charge movement following excitation to the FC S_1 state and relaxation to the equilibrium T_1 state. The upper curve was obtained from calculated $\Delta E_{ST} = E(S_0 \rightarrow S_1) - E(S_0 \rightarrow T_1)$. Both energies were obtained from TDDFT calculations on the equilibrium ground state geometry and include instantaneous reaction field contributions. The calculated ΔE_{ST} assumes no conformation change or time-dependent solvent contributions. The lower curve is a plot using experimental ΔE_{ST}. Both data sets fit to a concave-downward parabolic function and the calculated ΔE_{ST} is approximately 0.4 eV larger than the experimental value. The

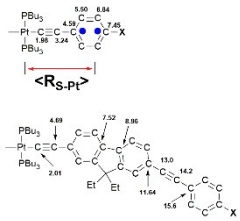

Chart 3 Example $\langle R_{S\text{-}Pt}\rangle$ distances for the **X** and **Fl-X** ligands. The red arrow shows $\langle R_{S\text{-}Pt}\rangle$ is a spin-weighted average distance from the TC to the central platinum atom.

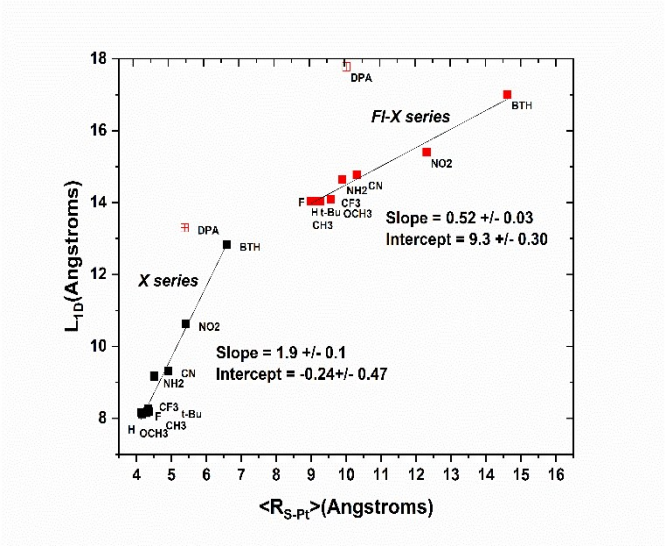

Fig. 6 Plot of L_{1D} calculated from Eqn. 5 as a function of $\langle R_{S\text{-}Pt}\rangle$.

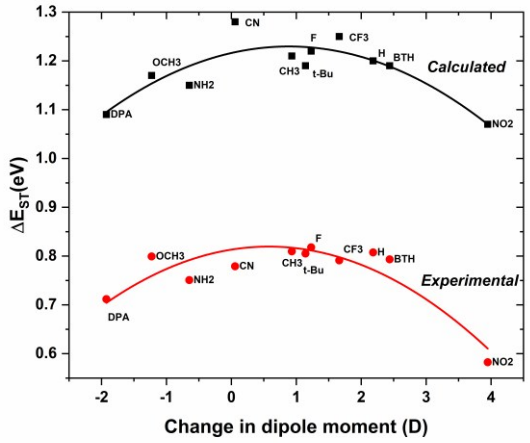

Fig`7 Plot of ΔE_{ST} vs calculated dipole moment change, $\Delta\mu = \mu_T - \Delta\mu_{01}$ where μ_T is the calculated equilibrium T_1 state dipole moment and $\Delta\mu_{01}$ is the calculated difference between the ground state and S_1 state dipole moments. The top curve is the energy difference $\Delta E_{ST} = E(S_0 - S_1) - E(S_0\text{-}T_1)$ obtained from TDDFT calculations using ground state geometry(Table 2). The top fitted curve is ΔE_{ST}(calculated, eV) = 1.22 + 0.03$\Delta\mu$ – 0.017$\Delta\mu^2$, r^2 = 0.72. The bottom curve is the corresponding plot from experimental data(Table 1). The bottom fitted curve is ΔE_{ST}(experimental, eV) = 0.81 + 0.02$\Delta\mu$ – 0.018$\Delta\mu^2$, r^2 = 0.78.

contributions to ΔE_{ST}include the exchange integral K_{01} obtained from TDDFT calculations($2K_{01}$ = $E(S_0 \rightarrow S_1) - E(S_0 \rightarrow T_1)$) as well as instantaneous solvent reaction field. Contributions to ΔE_{ST} also include time-dependent intramolecular and solvent cavity energy changes associated with FC excitation to the S_1 state having a dipole moment change from the ground state $\Delta\mu_{01}$ followed by intersystem crossing and relaxation to the equilibrium T_1 state having dipole moment μ_T. The 0.4 eV difference results from solvent and conformation effects as well as systematic errors from the DFT calculations.

The calculated $\Delta\mu_{01} > \mu_T$ in NH_2, OCH_3 and DPA implies instantaneous charge movement from the ligand to the central platinum forming the LMCT S_1 state, followed by time-dependent relaxation to a less polar equilibrium T_1 state. The calculated $\mu_T > \Delta\mu_{01}$ seen in BTH and NO_2 implies instantaneous charge movement from the central platinum atom to the ligand forming the MLCT S_1 state, followed by time-dependent relaxation to a more polar biradicaloid equilibrium T_1 state. The largest ΔE_{ST} values are associated with nonpolar end caps and smaller dipoles. The smallest ΔE_{ST} values in **NO_2** and **DPA** are associated with charge transfer after initial excitation end caps and dipole-dipole interaction with the polar solvent glass. The differences can be explained as the Hamiltonian for the exchange integral is $1/r_{12}$, and charge-separated states will have less electron correlation and more interaction with the polar solvent environment.

To determine T_1 state ΔPES relative to the ground state we assumed the displaced harmonic oscillator model[37,38] and calculated bond length changes relative to the ground state. Assuming small ΔPES, the Huang-Rhys factor *S* is a dimensionless parameter given by

$$\frac{I_{10}}{I_{00}} = S^2 = \frac{M\omega}{2\hbar}(\Delta R_e)^2 \qquad (6)$$

where I_{10} is the intensity of the 1-0 vibronic peak, I_{00} is the intensity of the 0-0 band normalized to 1, $\hbar$ = 1.054 x 10^{-34} J-s, *M* is the reduced mass in kg/atom associated with a vibration frequency $\omega(=c\nu)$ and ΔR_e is the equilibrium ΔPES associated with the T_1 state relative to the S_0 state. The ΔPES was calculated from Eqn. 6, assuming *M* = 12 amu, ω = 2,100 cm^{-1} and the Huang-Rhys factor measured from the emission spectrum intensity at 2,100 cm^{-1}. We were unable to estimate *S* from **NO_2**.

In the upper panel of Fig. 8 ΔPES is associated with increase in the C≡C bond length and decrease in Pt-C≡C and C≡C-C bond lengths. The smallest offset is associated with ED or EW ligands like **BTH**, **NH_2** and **DPA** while largest offsets are associated with neutral end caps like **CH_3**, **H** and **F**. This result is consistent with **BTH**'s TC being localized on the benzothiazole group rather than PA. The lower panel of Fig 8 shows $<R_{S\text{-}Pt}>$ is a function of ΔPES. A larger ΔPES is associated with a TC near the central platinum atom, while a smaller ΔPES is associated with a TC further away from the central platinum atom.

We were able to obtain triplet state absorption spectra from **DPA**, **CN**, **BTH** and **NO_2**(Figs S13-S18). The spectra exhibited broad-band transient absorption from 500-800 nm. Due to their red-shifted absorption spectra, we were able to examine the triplet state spectra

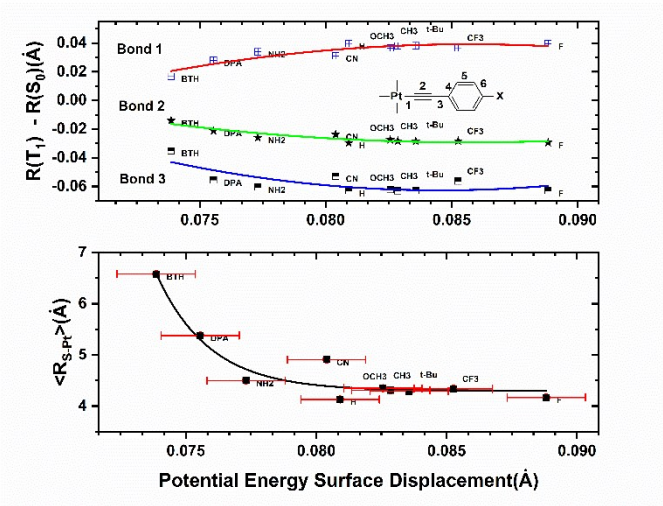

Fig. **8** Upper panel: Plot of bond length change(ΔR = R(T_1) – R(S_0) vs T_1-S_0 state ΔPES. ΔPES was calculated from equation 6 assuming M = 12 amu, ω = 2,100 cm^{-1} and the Huang-Rhys factor measured from the emission spectrum intensity at 2,100 cm^{-1}(Table 1); Lower panel: plot of $<R_{S\text{-}Pt}>$ vs T_1-S_0 state PES displacement.

of **BTH** and **NO_2** via fs transient absorption in benzene with 400 nm excitation(Fig 9). At time zero **BTH**(upper panel, Fig. 9) has peaks at

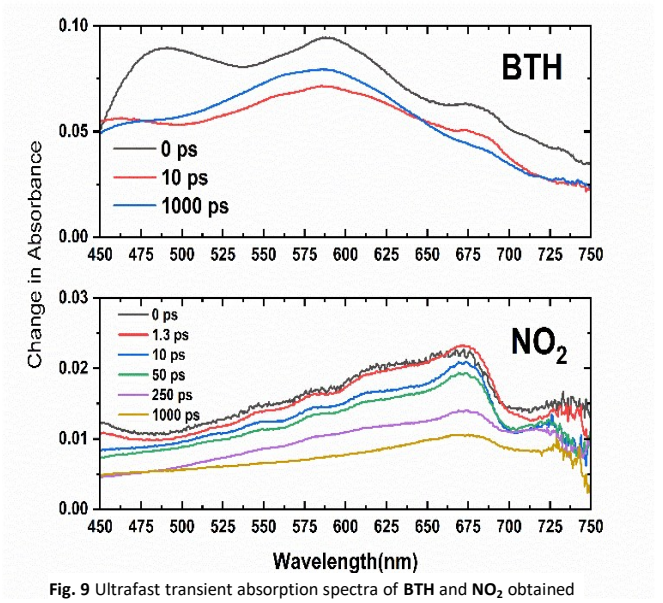

Fig. 9 Ultrafast transient absorption spectra of **BTH** and **NO_2** obtained from THF solutions at room temperature.

490, 586, and 676 nm. By 10 ps the 490 nm peak has essentially disappeared while the other two persist, but decrease in intensity. This short lifetime is 2.40 +/- 0.85 ps is attributed to intramolecular vibration and solvent relaxation. The peak at 490 nm may also be associated with instantaneous charge transfer from the central platinum atom to the ligand, forming the FC MLCT S_1 state. Its decay may be associated with formation of the more polar biradicaloid equilibrium T_1 state. From this point there is an increase in ΔOD at the maximum with an observed lifetime of 486 +/- 27 ps. There is a slight blue shift of the max to 490 nm while the shoulder at 676 nm is significantly less pronounced. This spectrum resembles the T_1 state so this process is assigned as intersystem crossing. The electron density in the S_1 state of **BTH** is likely more distal to the Pt center, slowing intersystem crossing. At time zero **NO_2** (lower panel, Fig.

9)has a higher energy peak/shoulder near 610 nm. It decays with a lifetime of 5.79 +/- 1.13 ps attributed to a combination of vibrational cooling and solvent relaxation leading to a peak around 665-670 nm. The spectrum around 10 ps also has some shoulders/structure at higher energy, which then decay to leave just a broad, featureless spectrum with an absorption maximum in the 665-670 nm range. A long decay with a 242 +/- 12 ps lifetime is attributed to intersystem crossing. For comparison, compound **H** has a <100 fs intersystem crossing lifetime and 4.1 ps solvent relaxation component.[23] The MLCT character and movement of charge away from the central platinum of the **BTH** and **NO_2** S_1 states during ISC compared to **H** gives evidence for weaker SOC in the triplet states of **BTH** and **NO_2**.

To estimate the electronic contribution to the triplet state lifetime, we used the energy gap law for the nonradiative decay rate constant.[39] The energy gap law is the product of two terms: a spin-orbit coupling(SOC) term, V_{SOC}^2 and an energy gap term, $EG(E_T)$.

$$k_{nr} = \frac{V_{SOC}{}^2\sqrt{2\pi}}{\hbar\sqrt{\hbar\omega E_T}} \exp\left(\frac{-\gamma E_T}{\hbar\omega}\right) = V_{SOC}^2\, EG(E_T)\,, \qquad (7)$$

where E_T is the $T_1 - S_0$ energy gap, $\hbar\boldsymbol{\omega}$ is the energy of the acceptor vibration mode, γ is a function of molecular parameters and $V_{SOC} = \langle T_1|H|S_0\rangle$ is the electronic matrix element accounting for SOC and other electronic interactions. To calculate V_{SOC}, we assume $k_{nr} >> k_r$, γ~1, and $\hbar\boldsymbol{\omega}$ = 3,000 cm^{-1} corresponding to C-H stretch vibrations. Fig. 10 is a plot of the estimated electronic matrix element V_{SOC} *vs.* $<R_{S\text{-}Pt}>$ for both series of chromophores. The plot shows strong spin-orbit coupling between the TC and the platinum atom at a range $<R_{S\text{-}Pt}> < 6$ *Å*. Rapid triplet decay is associated with the triplet state being confined to PA, while slower triplet decay is associated with the triplet state being on both PA and the end cap. In series **X** going from **H** to **NO_2**, k_{nr}***(H)***$/k_{nr}$***(NO_2)*** *= 33,000*. Most of the variation in k_{nr} results from spin orbit coupling as V_{SOC}***(H)***$/V_{SOC}$***(NO_2)*** *= 366* while the *EG(**H**)/EG(**NO_2**) = 0.25*. The variation in k_{nr} results from the V_{SOC} term rather than the *EG* term. In contrast, there are published measurements of k_{nr} for a series of platinum acetylides having E_T values down to 1.30 eV.[40] In that series k_{nr}*(high)*$/k_{nr}$*(low) = 125*, V_{SOC}(high)/V_{SOC}(low) = 1.9, while *EG(high)/EG(low) = 33*. Due to the lower triplet energies, the variation in k_{nr} from this data set results from the EG term rather than the V_{SOC} term.

Conclusions

This study has focused on the use of descriptors derived from DFT calculations to understand the triplet state behavior of a systematic series of platinum acetylides. We found that E_T is a good estimate of the 0-0 band energy obtained from phosphorescence spectra. The energy measures emission from the T_1 state, which is confined to one ligand. Higher energy states will be associated with the other ligand.[41] The spin density on the end cap, *SD(**X**)*, is a quadratic function of the S_1 state electron density change on the platinum atom associated with MLCT or LMCT states. We also show that *SD(**X**)* is a function of PA bond length changes, where the bond length change is larger with ED substituents and smaller with EW substituents. Larger ΔPES values are associated with ED end caps and more PA distortion. Smaller ΔPES values are associated with EW end caps and less PA distortion.

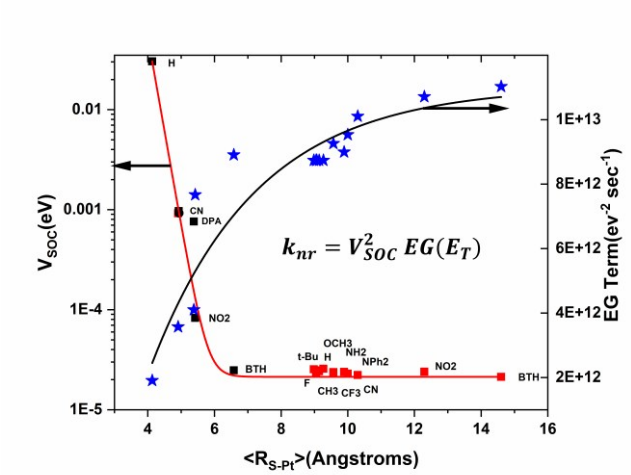

Fig. 10 Plot of the spin orbit coupling energy and energy gap term of series **X** and **Fl-X** as a function of $<R_{S\text{-}Pt}>$. Black data points were obtained from series **X**. Red data points were previously published for series **Fl-X**.(1). Blue data points were calculated from the EG term of the energy gap law(Eqn. 8).

The descriptor $<R_{S\text{-}Pt}>$ measures the distance between the TC and the central platinum atom. By combining data from both the **X** and published **Fl-X** series, the energy gap law shows the variation of triplet decay rate constant results from strong short range SOC interaction between the triplet state and the central platinum and a weaker contribution from the energy gap term. The SOC interaction is larger with ED substituents and smaller with EW substituents. The one-dimensional well length $L_{1D} > <R_{S\text{-}Pt}>$, giving evidence for confinement of the TC. Also, the effect of end cap on $<R_{S\text{-}Pt}>$ is less in the **Fl-X** series compared to the **X** series. The TC concept could be useful in studying the behavior of Frenkel excitons, defined to be tightly-bound electron-hole pairs of molecular dimension located in molecular crystals. Frenkel excitons are involved in singlet fission and triplet fusion processes.[42] Although we successfully calculated E_T with TDDFT methods(Fig. 1D), visualizing the triplet excited state as a point may be useful in understanding triplet mobility in polymers and molecular crystals.

Machine learning algorithms are a strategy to screen large numbers of candidate materials towards a goal.[43,44] A recent publication demonstrated a search for chromophore structures having a target S_1 state energy.[16] Their strategy involves the use of molecular structure generation software followed by DFT calculations of the S_1 state energy to produce possible structures rated according to a "reward function". The authors synthesized several optimum candidates and the calculations show good agreement with experiment. The current work gives descriptors that could be used in a machine learning project to search for platinum acetylides with desired photophysical properties such as triplet energy from E_T calculations and lifetime from $<R_{S\text{-}Pt}>$ calculations.[45-48]

Conflicts of Interest

There are no conflicts to declare.

Acknowledgements

We thank the support of this work by AFRL/RX contracts F33615-03-D-5408 for D.M.K. and A.R.B. F33615-03-D-5421 for J.E.S. and FA9550-09-1-0219 for A.R.B.; We thank Abigail Shelton from the Shanze group, University of Florida, for collection of phosphorescence spectra and Tod Grusenmeyer for insights in analyzing phosphorescence bandshape. We thank the referees for very helpful comments and suggestions.

Notes and references

1 J. E. Haley, D. M. Krein, J. L. Monahan, A. R. Burke, D. G. McLean, J. E. Slagle, A. Fratini, T. M. Cooper,. *J. Phys. Chem. A*, 2011, **113**, 265.
2 J. E. Rogers, J. E. Slagle, D. M. Krein, A. R. Burke, B. C. Hall, A. Fratini , D. G. McLean, P. A. Fleitz, T. M. Cooper, M. Drobizhev, A. Rebane, *Inorg. Chem*., 2007, **46**, 6483.
3 G. S. He, L.-S. Tan, Q. Zheng, P. N. Prasad, *Chem. Rev.*, 2008, **108**, 1245.
4 S. R. Marder, C. B. Gorman, F. Meyers, J. W. Perry, G. Bourhill, B J.-L. Bredas, B. M. Pierce, *Science*, 1994, **265**, 632.
5 D. Lu, G. Chen, J. W. Perry, W. A. Goddard, *J. Am. Chem Soc.*, 1994, **116**, 10679.
6 C. Liao, A. H. Shelton, K.-Y. Kim, K. S. Schanze, *ACS Appl. Mater. Interfaces*, 2011, **3**, 3225.
7 R. A. Haque, Al-Balushi, I. J. Al-Busaidi, M. S. Khan, P. R. Raithby, *Chem. Rev,* 2018, **118**, 8474.
8 A. H. Shelton, S. R. Valandro, R. S. Price, G. G. Dubinina, K. A. Abboud, G. Wicks, A. Rebane, M. Younus, K. S. Schanze, *J. Phys. Chem. A, 2019*, **123**, 9382.
9 T. M. Cooper, D. M. Krein, A. R. Burke, D. G. McLean, J. E. Rogers, J. E. Slagle, *J. Phys. Chem. A*, 2006, **110**, 13370.
10 W. M. Berhanu, G. G. Pillai, A. A. Oliferenko, A. R. Katritzky, *ChemPlusChem*, 2012, **77**, 507.
11 P. K. Chattaraj, D. R. Roy, *Chem. Rev.*, 2007, **107**, PR46.
12 A. Rebane, M. Drobizhev, N. S. Makarov, G. Wicks, P. Wnuk, Y. Stepanenko, J. E. Haley, D. M. Krein, J. E. Fore, A. R. Burke, J. E. slagle, D. G. McLean, T. M. Cooper, *J. Phys. Chem. A*, 2014, **118**, 3749.
13 A. Rebane, M. Drobizhev, N. S. Makarov, E. Beuerman, J. E. Haley, D. M. Krein, et al., *J. Phys. Chem. A*, 2011, **115**, 4255.
14 T. M. Cooper, J. E. Haley, D. M. Krein, A. R. Burke, J. E. Slagle, A. Mikhailov, A. Rebane, *J. Phys. Chem. A*, 2017, **121**, 5442.
15 G. Baryshnikov, B. Minaev, H. Agren, *Chem. Rev*., 2017, **117**, 6500.
16 M. Sumita, X. Yang, S. Ishihara, R. Tamura, K. Tsuda, *ACS Central Science*, 2018, **4**, 1126.
17 G. Angulo, G. Grampp, A. Rosspeintner, *Spectrochimica Acta Part A*, 2006, **65**, 727.
18 J. E. Rogers, T. M. Cooper, P. A. Fleitz, D. J. Glass, D. G. McLean, *J. Phys. Chem. A*, 2002, **106**, 10108.
19 A. V. Nikolaitchik, O. Korth, M. A. J. Rodgers, *J. Phys. Chem. A*, 1999, **103**, 7587.
20 Gaussian 09, Revision E.01, M. J. Frisch, G. W. Trucks, H. B. Schlegel, G. E. Scuseria, M. A. Robb, J. R. Cheeseman, G. Scalmani, V. Barone, B. Mennucci, G. A. Petersson, H. Nakatsuji, M. Caricato, X. Li, H. P. Hratchian, A. F. Izmaylov, J. Bloino, G. Zheng, J. L. Sonnenberg, M. Hada, M. Ehara, K. Toyota, R. Fukuda, J. Hasegawa, M. Ishida, T. Nakajima, Y. Honda, O. Kitao, H. Nakai, T. Vreven, J. A. Montgomery, Jr., J. E. Peralta, F. Ogliaro, M. Bearpark, J. J. Heyd, E. Brothers, K. N. Kudin, V. N. Staroverov, T. Keith, R. Kobayashi, J. Normand, K. Raghavachari, A. Rendell, J. C. Burant, S. S. Iyengar, J. Tomasi, M. Cossi, N. Rega, J. M. Millam, M. Klene, J. E. Knox, J. B. Cross, V. Bakken, C. Adamo, J. Jaramillo, R. Gomperts, R. E. Stratmann, O. Yazyev, A. J. Austin, R. Cammi, C. Pomelli, J. W. Ochterski, R. L. Martin, K. Morokuma, V. G. Zakrzewski, G. A. Voth, P. Salvador, J. J. Dannenberg, S. Dapprich, A. D. Daniels, O. Farkas, J. B. Foresman, J. V. Ortiz, J. Cioslowski, and D. J. Fox, Gaussian, Inc., Wallingford CT, 2013.
21 G. Scalmani, M. J. Frisch, B. Mennucci, J. Tomasi, R. Cammi, V. Barone, *J. Chem. Phys*., 2006, **124**, 94107.
22 T. Yanai, D. Tew, N. Handy, *Chem. Phys. Lett*., 2004, **393**, 51.
23 G. Ramakrishna, T. Goodson III, J. E. Rogers-Haley, T. M. Cooper, D. G. McLean, A. Urbas, *J. Phys. Chem. C,* 2009, **113**, 1060.
24 A. A. I. Sina, S. M. I. Al-Rafia, M. F. Ahmad, R. K. Paul, S. M. S. Islam, M. Younus, et al., *J. Inorg. and Organomet. Poly. Mater.*, 2015, **25**, 427.
25 Y. Nagano, T. Ikoma, K. Akiyama, S. Tero-Kubota, *Chem. Phys. Lett*., 1999, **303**, 201.
26 R. J. Magyar, S. Tretiak, Y. Gao, H.-L. Wang, A. P. Shreve, *Chem. Phys. Lett.*, 2005, **401**, 149.
27 M. Soderberg, B. Dereka, A. Marrocchi, B. Carlotti, E. Vauthey, *J. Phys. Chem. Lett.,* 2019, **10**, 2944.
28 J. Sjoqvist, M. Linares, P. Norman, *J. Phys. Chem. A*, 2010, **114**, 4981.
29 T. Chen, L. Zheng, J. Yuan, Z. An, R. Chen, Y. Tao, H. Li, X. Xie, W. Huang, *Sci. Rep*., 2015, **5**, 10923.
30 T. M. Cooper, D. M. Krein, A. R. Burke, D. G. McLean, J. E. Rogers, J. E. Slagle, P. A. Fleitz, *J. Phys. Chem. A*, 2006, **110**, 4369.
31 M. G. Kuzyk, *Size*, Create Space Publishing, 2017.
32 B. D. Anderson, *J. Chem. Ed.*, 1997, **74**, 985.
33 M. De Giorgi, M. Tari, L. Manna, R. Cingolani, *Microelect. J.*, 2005, **36,** 552.
34 L. Brus, *J. Phys. Chem.*, 1986, **90**, 2555.
35 G. Baldacchini, In: B. Di Bartolo, ed., NATO ASI Series B. 301, New York, Plenum Press, 1992, 255.
36 M. Fox, *Optical Properties of Solids*, Oxford, Oxford University Press, 2010.
37 Y. Fujimura, K. Sato, T. Nakajima, A displaced harmonic oscillator model for the time-resolved emission spectra, *Bull. Chem. Soc. Jpn*., 1982, **55**, 277.
38 G. C. Schatz, M. A. Ratner, *Quantum Mechanics in Chemistry*, Dover Publications, 2002.
39 R. Englman, J. Jortner, *Mol. Phys.*, 1970, **18**, 145.
40 J. S. Wilson, N. Chawdhury, M. R. A. Al-Mandhary, M. Younus, M. S. Khan, P. R. Raithby, A. Kohler, R. H. Friend, *J. Am. Chem Soc.*, 2001, **123**, 9412.
41 A. Canaguier-Durand, E. Devaux, J. George, Y. Pang, J. A. Hutchison, T. Schwartz, et al., *Angew. Chem*., 2013, **52**, 10533.
42 A. Matsui, H. Nishimura, *J. Phys. Soc. Jpn.*, 1980, **49**, 657.
43 G. B. Goh, N. O. Hodas, A, Vishnu, *J. Comp. Chem*., 2017, **38**, 1291.
44 K. Tran, A. Palizhati, S. Back, Z.W. Ulissi, *J. Chem. Inf. Mod*., 2018, **58**, 2392.
45 Z. An, C. Zheng, Y. Tao, R. Chen, H. Shi, T. Chen, Z. Wang, H. Li, R. Deng, X. Liu, W. Huang, *Nature Mater*., 2014, **14**, 685.
46 W. Zhao, Z. He, J. W. Y. Lam, Q. Peng, H. Ma, Z. Shuai, G. Bai, J. Hao, B. Z. Tang, *Chem.* 2016, **1**, 592.

47 S. Hirata, M. Vacha, *Adv. Opt. Mater.*, 2015, 1.
48 S. Xu, R. Chen, C. Zheng, W. Huang, *Adv. Mater.*, 2016, **28**, 9920.

Ligand end cap **X** determines triplet state behavior.